







RESEARCH ARTICLE

10.1002/2016MS000764

Closing the scale gap between land surface parameterizations and GCMs with a new scheme, SiB3-Bins

I. T. Baker¹ , P. J. Sellers² , A. S. Denning¹, I. Medina¹ , P. Kraus¹, K. D. Haynes¹ , and S. C. Biraud³

¹Colorado State University, Atmospheric Science Department, Fort Collins, Colorado, USA, ²Deceased 23 December 2016; Formerly NASA Goddard Space Flight Center, ³Lawrence Berkeley National Laboratory, Berkeley, California, USA

Key Points:

- Soil moisture is a strong regulator of evapotranspiration (ET), and varies on spatial scales much smaller than atmospheric model grid cells
- We present a method to account for subgrid scale variability, using wetness bins of variable area to relate soil moisture to ET
- In a test against tower flux data, this new method performs well in regions where soils transition from wet to dry during the seasonal cycle

Correspondence to:

I. T. Baker,
baker@atmos.colostate.edu

Citation:

Baker, I. T., P. J. Sellers, A. S. Denning, I. Medina, P. Kraus, K. D. Haynes, and S. C. Biraud (2017), Closing the scale gap between land surface parameterizations and GCMs with a new scheme, SiB3-Bins, *J. Adv. Model. Earth Syst.*, 9, doi:10.1002/2016MS000764.

Received 19 JUL 2016

Accepted 9 FEB 2017

Accepted article online 15 FEB 2017

© 2017. The Authors.

This is an open access article under the terms of the Creative Commons Attribution-NonCommercial-NoDerivs License, which permits use and distribution in any medium, provided the original work is properly cited, the use is non-commercial and no modifications or adaptations are made.

Abstract The interaction of land with the atmosphere is sensitive to soil moisture (W). Evapotranspiration (ET) reacts to soil moisture in a nonlinear way, $f(W)$, as soils dry from saturation to wilt point. This nonlinear behavior and the fact that soil moisture varies on scales as small as 1–10 m in nature, while numerical general circulation models (GCMs) have grid cell sizes on the order of 1 to 100s of kilometers, makes the calculation of grid cell-average ET problematic. It is impractical to simulate the land in GCMs on the small scales seen in nature, so techniques have been developed to represent subgrid scale heterogeneity, including: (1) statistical-dynamical representations of grid subelements of varying wetness, (2) relaxation of $f(W)$, (3) moderating $f(W)$ with approximations of catchment hydrology, (4) “tiling” the landscape into vegetation types, and (5) hyperresolution. Here we present an alternative method for representing subgrid variability in W , one proven in a conceptual framework where landscape-scale W is represented as a series of “Bins” of increasing wetness from dry to saturated. The grid cell-level $f(W)$ is defined by the integral of the fractional area of the wetness bins and the value of $f(W)$ associated with each. This approach accounts for the spatio-temporal dynamics of W . We implemented this approach in the SiB3 land surface parameterization and then evaluated its performance against a control, which assumes a horizontally uniform field of W . We demonstrate that the Bins method, with a physical basis, attenuates unrealistic jumps in model state and ET seen in the control runs.

1. Introduction

1.1. Land-Atmosphere Coupling, Soil Moisture Importance

The atmosphere and land surface are bidirectionally coupled [e.g., Charney, 1975; Shukla and Mintz, 1982; Entekhabi et al., 1996; Sellers et al., 1997; Koster et al., 2004; Seneviratne et al., 2010; Gentine et al., 2012]. Incoming radiation, precipitation, wind, temperature, and humidity influence the surface, while surface conditions interact with these same variables to determine the fluxes of energy, moisture, momentum, and trace gases between the atmosphere and the terrestrial biosphere. Global-scale general circulation models (GCMs) of the atmosphere have had persistent challenges in realistically calculating these fluxes [Sellers et al., 1996c; Pitman, 2003; Yang, 2004].

Surface fluxes are closely coupled to land surface conditions (slope, vegetation, and soil moisture) that vary widely on length scales of 1 m to many kilometers. In contrast, most GCMs have spatial resolutions of 25–200 km, but require accurate grid-averaged surface-atmosphere fluxes, as calculated by their land surface parameterizations (LSPs), to predict the future state of the atmosphere, including cloudiness and rainfall, which in turn feedback directly onto the land surface condition [Sato et al., 1989; Koster et al., 2006; Santanello and Peters-Lidard, 2011]. Bridging this scale gap explicitly by increasing the resolution of GCMs to the scale of surface heterogeneity is not practical.

The scale gap has to be confronted directly with improved parameterizations, whatever the resolution of the GCM. This means that credible (i.e., verifiable) new LSPs must be developed and tested offline and in GCMs. Entekhabi and Eagleson [1989], Sellers et al. [1992a], Georgi and Avissar [1997], and Nakaegawa et al. [2000] have all shown how the scale gap could be a problem for different land surface processes in GCMs. The numerical tests of Sellers et al. [1992a] assumed that the lower atmospheric forcing (downwelling radiation, temperature, humidity, wind speed) is relatively homogeneous over a grid area at a given time, but

interacts with a surface of spatially varying slope, vegetation density, and soil wetness. However, soil moisture, with its much greater spatial variability [Schmugge and Jackson, 1996; Ryu and Famiglietti, 2006] and its associated nonlinear relationships to evapotranspiration, does not lend itself to simple integration. Soil moisture and the processes that depend on it are significant hold-outs against bridging the scale gap.

In this paper, we explore a new methodology, the Bins approach of Sellers et al. [2007] (hereafter, SE07), for representing soil moisture heterogeneity in a commonly used LSP, SiB3 [Baker et al., 2003, 2008]. We will demonstrate that this technique can effectively bridge the scale gap for soil moisture in GCMs and has the potential to improve the calculation of surface-atmosphere fluxes of heat, water vapor, and trace gases, especially in highly seasonal or semiarid regions where robust and realistic simulations have proven to be difficult [Schwalm et al., 2010].

1.2. Soil Moisture Regulation of Transpiration

Evapotranspiration (ET) is nonlinearly related to soil moisture. Early work such as Pierce [1958], Lowry [1959], and Budyko [1974] describe empirical curves relating the decrease in ET as soils dry out. Canopy density, seasonality, and phenology influence the partition between soil surface evaporation and transpiration. As wet soils dry, water becomes more tightly bound to soil particles, until a threshold is reached (wilt point) where moisture becomes virtually inaccessible to roots. Plant-scale observations reveal this process to be very nonlinear. Plants will function normally as soil moisture is reduced, then close their stomates rapidly as the wilt point is approached, as shown in Figure 1 [Muchow and Sinclair, 1991; Colello et al., 1998; Serraj et al., 1999; Laio et al., 2001b]. Individual plants use hormones to communicate between their root systems, where water stress is sensed, to their stomates, which explains this sharp “On-Off” response to decreasing soil moisture [Kim et al., 2010]. We represent this behavior (as in SE07) as:

$$E = E_p f(W) \tag{1}$$

where E is the transpiration rate, E_p is the potential unstressed transpiration rate, W is soil moisture expressed as fraction of saturation, and $f(W)$ describes the effect of soil moisture stress, ranging from 1 when the soil is wet to 0 at wilt point when high surface tension within the soil prevents transpiration.

SE07 demonstrated that using equation (1) to describe the evapotranspiration (soil evaporation and transpiration were considered as a single process) response of the entire grid square was unrealistic. This is easy to understand: within a given grid square, individual plants will transition from on to off per equation (1) as

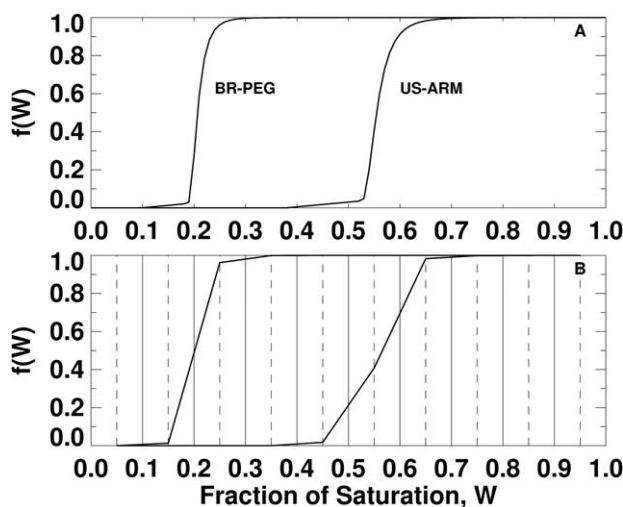


Figure 1. Relationship between soil saturation fraction W and stress function $f(W)$. This describes the ability of roots to extract water from the soil. A value of 1 implies no stress, and a value of 0 results in shutdown of ET. Two sites are shown: Pe de Gigante, São Paulo State, Brazil (BR-PEG; 85% sand, 3% clay) and ARM Southern Great Plains tallgrass site in Oklahoma, USA (US-ARM; 37% sand, 23% clay). (a) The “continuous” value of $f(W)$ and (b) the curve of $f(W)$ when discretized into 10 bins.

the local soil moisture content decreases, but a potential range of soil moisture conditions within a grid area may result in a modulated, i.e., less steep, integrated response for the landscape as a whole. Across a landscape of size similar to a GCM grid cell (~100 km) soil moisture varies as a result of topographic position, as locations higher on hillslopes will be drier, while lower, riparian regions will be wetter or saturated. Precipitation can reduce heterogeneity through stratiform rainfall that moistens the entire domain, or soil wetness heterogeneity independent of topographic position can be increased by migrating convective cells. Finally, preferential ET from wetter regions in the absence of rainfall will result in large-scale drying and reduction of heterogeneity [Sellers et al., 1992a, 1995; Pan et al., 2008; Li and Rodell, 2013], although this behavior is not observed universally [e.g., Famiglietti et al., 1999; Teuling et al., 2007; Liu et al., 2012].

Subgrid heterogeneity can be approximated by a variety of methods. Some of these methods include:

1. Statistical-dynamical treatments: Several models use different statistical methods to generate descriptions of spatial variability in soil moisture. *Entekhabi and Eagleson* [1989] use a two-parameter gamma function to describe spatial variability of soil moisture, then derive equations for infiltration-excess (Horton) and saturation-excess (Dunne) surface runoff (subsurface runoff is not considered). Equations are derived for evaporative loss of water from surface soil and for removal of water from the soil column via transpiration, with subgrid variability again determined by the character of the gamma function. Bare-soil evaporation is determined by the balance between gravitational drainage and diffusivity (upward) along a moisture gradient. The authors describe the ET from wet soils as being controlled by the atmospheric potential, ET in dry conditions controlled by the soil (water limited), and they define a soil moisture value (s^*) that describes the boundary between these two regimes. There is no soil restriction (analogous to $f(W) = 1$) where soil moisture exceeds s^* , and a linear reduction in $f(W)$ between s^* and wilt point, where $f(W) = 0$. Evaporation from the soil surface is controlled directly by gravitational, diffusive, and capillary forces, as opposed to the empirical resistance formulation favored by some others [i.e., *Sellers et al.*, 1986, 1996a; *Colello et al.*, 1998].

Wood et al. [1988] introduce the idea of a Representative Elemental Area (REA) as a size dimension that is large enough so that a statistical representation is adequate to capture spatial variability, and explicit modeling of heterogeneity is not required. Using this idea, *Famiglietti and Wood* [1994a] construct a model where hydrologic regimes are defined and use topographic data following TOPMODEL (TOPography-based hydrological MODEL) [*Beven and Kirkby*, 1979; *Sivapalan*, 1987] where water table depth decreases (and ET approaches potential values) along a gradient from upland to riparian regions. In these “interacting buckets” there is no between-element water transfer in the unsaturated zone, but saturated subsurface flow can move between elements. In an application to a tallgrass prairie [*Famiglietti and Wood*, 1994b] they find that this statistical representation gives results almost identical to a high-resolution explicit treatment.

Motivated by improving runoff simulation, *Koster et al.* [2000] also use TOPMODEL topographic index to characterize the statistical-dynamical characteristics of individual catchments within a grid cell, then partition this catchment into three distinct regimes (saturated, transpiration, and wilting). Catchment-scale topographic index data determines a shape pdf relating area to mean water table depth (\bar{d}), and adjustment in \bar{d} determines the relative area of the three regimes within each catchment.

These treatments are similar in that topographical information plays a leading role in determining statistics and treatment of heterogeneity within a grid cell. Spatial variability of precipitation is not considered. In most cases, the shape of the density function relating wetness and relative area are assumed, based on either topography or on representative catchment-scale moisture values.

2. Relaxation: Equation (1) is “relaxed” when inserted into the GCM LSP, by flattening out the $f(W)$ curve, using the assumption that landscape-scale processes will incorporate a range of W values in the domain [e.g., *Laio et al.*, 2001a; *Porporato et al.*, 2001, 2002; *Rodriguez-Iturbe*, 2000; *Baker et al.*, 2008, 2013]. This leads to more graceful dry-downs, but it does not have a sound biophysical basis.
3. Catchment hydrology: *Wood et al.* [1992] proposed a modified catchment model with a treatment of variable infiltration capacity (VIC) over the grid area to moderate the effects of equation (1). The model did not directly address vegetation effects but describes the effects of a varying saturated area which contributes to direct runoff. Model tests showed improved performance over conventional bucket models [e.g., *Budyko*, 1974], but the approach has limitations for the calculation of surface-atmosphere fluxes in that there are no explicit physiological controls on ET.
4. Tiling: Another approach is to aggregate subgrid areas with common characteristics, usually vegetation type [*Avisar and Pielke*, 1989; *Koster and Suarez*, 1992; *Bonan et al.*, 2002; *Ke et al.*, 2013]. In this case, soil moisture heterogeneity is implicitly coupled to vegetation. Surface-atmosphere fluxes are calculated separately for the tiles within a grid-area and multiplied by fractional area to provide the area-weighted flux. This approach is used in some biophysical LSPs [e.g., *Koster and Suarez*, 1992; *Bonan et al.*, 2002; *Krinner et al.*, 2005; *Arain et al.*, 2006; *Best et al.*, 2011]. SE07 divided a grid cell of uniform vegetation content into tiles and demonstrated that tiling has its own numerical and accuracy problems, including large excursions from “reality” (as defined by a very high resolution calculation using 10^6 cells) unless a very large number of tiles are used. *Medina et al.* [2014] demonstrated that 10 tiles were able to capture the variability represented by 100 grid cells over an arbitrary area, in an application of SE07.

5. Hyperresolution: This approach relies on explicit simulation at very high spatial resolution ($\sim 10\text{--}100$ m) to deal with all possible combinations of topography, vegetation, and soil moisture [Wood *et al.*, 2011]. This may be computationally possible in the GCM environment at some point in the future, but the arguments for it have been disputed [Beven and Cloke, 2012]. The problems of parameter specification and computational expense would be immense, and the benefits doubtful. Parameterizations would still have to be used and the computational resources might be better spent on ensemble runs at coarser resolution.

With no single solution, the problem remains. Here we expand the concepts of SE07 into a “full” model, to calculate realistic and accurate grid-averaged fluxes at reasonable cost, while accounting for the time-space variations of the independent surface variables.

1.3. Soil Wetness Bins

A conceptual method was introduced in SE07 to represent subgrid variability of soil moisture and its influence on ET, using an extremely simple model based on equation (1). In this treatment, domain-scale soil moisture is represented as a distribution, whereby soil wetness (from dry to saturated) is discretized into a finite number of “Bins,” each associated with a fraction of the grid area. The midpoint wetness value of each bin defines the representative wetness function controlling ET for that bin, as defined by equation (1). In SE07 the “Bins” method, as well as a calculation using domain-averaged wetness (a “control” simulation analogous to the method currently used in many GCMs today) was evaluated against an explicit representation of 10^6 individual calculations (which corresponded to “reality”) where soil moisture was allowed to evolve in response to variable conditions as might be experienced across a GCM grid cell. It was demonstrated that, especially at times when the domain-averaged wetness falls in the nonlinear region of $f(W)$, the “control” ET can experience large fluctuations as well as exhibit large errors when compared to the explicit method. The “Bins” method was shown to reduce errors considerably when compared with the explicit simulation and to track the “reality” case closely, even when using a small number of bins (such as 10). After each time step, the fractional areas associated with each bin are updated in accordance with their contributions to the ET rate, and thus the evolving dynamics of the spatial variability of soil moisture are captured over time. However, in the SE07 study, equation (1) only crudely represented all the complexities of soil moisture control on evapotranspiration; the soil model was a single layer, the time step was 1 day, and the meteorological forcing that controlled potential ET was invariant across time and space.

In this study, we apply the methods described in SE07 within the Simple Biosphere Model (SiB) [Sellers *et al.*, 1986, 1996a; Baker *et al.*, 2003, 2008] and test the resulting model in standalone mode at two semiarid field sites. We evaluate simulations of energy, moisture, and carbon flux between the land surface and atmosphere, and do so using a more realistic representation of the processes involved than was possible in SE07.

2. Methods

2.1. Simple Biosphere Model

The Simple Biosphere Model (SiB) was first introduced as an LSP for GCMs by Sellers *et al.* [1986]. It has since undergone several revisions: SiB2 [Sellers *et al.*, 1996a] and SiB3 [Baker *et al.*, 2003, 2008]. SiB2 and subsequent versions incorporate the “enzyme-kinetics” class of photosynthesis-conductance models following Farquhar *et al.* [1980], Ball *et al.* [1987], and Collatz *et al.* [1991, 1992] with integration up to the canopy scale and phenology specified by satellite data as described in Sellers *et al.* [1992b,b]. The SiB3 and SiB4 soil modules are now similar to the Common Land Model (CoLM) [Dai *et al.*, 2003] or the Community Land Model (CLM) [Lawrence *et al.*, 2011], in that moisture and temperature are collocated in the layers of the numerical scheme, an improvement from the initial SiB and SiB2 formulations which held soil moisture and temperature in mismatched layers.

SiB has been coupled to global GCMs [Sato *et al.*, 1989; Randall *et al.*, 1996; Sellers *et al.*, 1996c] as well as to mesoscale models [Denning *et al.*, 2002; Nicholls *et al.*, 2004; Wang *et al.*, 2007; Corbin *et al.*, 2008, 2010]. Evaluation against eddy-covariance fluxes at individual sites have been performed in forests [Baker *et al.*, 2003, 2008, 2013; Schaefer *et al.*, 2008] and grasslands [Colello *et al.*, 1998; Hanan *et al.*, 2005]. SiB has a demonstrated competence when compared with other land-atmosphere model across multiple sites [Schwalm *et al.*, 2010].

Previously, SiB has applied the “stress function,” $f(\langle W \rangle)$ (where $\langle \rangle$ represents the area-average value), to evaporation and photosynthesis by multiplying the unstressed canopy conductance term to yield the actual

canopy conductance, g_c [Sellers et al., 1996a]. The formulation for $f(W)$ used in this paper follows SE07, which is similar but not identical to the equation used in SiB2 [Sellers et al., 1996a] which was itself related to Colello et al. [1998]. The equation used in SE07 is

$$f(W) = \text{Max}(0.0; 0.25(W - 0.1); \tan h(0.0045\psi_s W^{-8}) + 1) \quad (2)$$

where ψ_s is the moisture potential in the soil at saturation and W is the fractional saturation of the soil. The dependence upon ψ_s shifts the region of large variability in $f(W)$ with respect to relative saturation as sand and clay content in the soil changes. Figure 1 shows examples of $f(W)$ for the two sites used in this study, Pe de Gigante in São Paulo state in Brazil (BR-PEG), and the US-ARM Southern Great Plains winter wheat site in Oklahoma, USA (US-ARM).

2.2. Bins Configuration and Numerical Scheme

That there is heterogeneity in soil moisture is axiomatic. The Bins paradigm is agnostic to whether that heterogeneity is due to topography, precipitation, or vegetation. In this regard, the Bins method is not a discretization of equations that describe actual physical processes such as overland or subsurface flow of water, but is

rather an abstraction. The bins are a physically consistent mathematical description that encompasses multiple ecophysiological processes.

We can use an example to illustrate this. In Figure 2, we demonstrate a drying sequence, moving from top to bottom. Moving from bottom to top could be a moistening sequence. The left hand column shows a single wetness value, as calculated using multiple layers in the vertical domain with a single value in each layer representing the entire grid cell. We call this Z-space. Initially (top plot), the vertically integrated column is moist. As runoff and ET remove water from the column, the wetness value decreases. This behavior may be thought of as homogeneous, where all area in the grid cell is described with a single wetness value that moves incrementally in response to wetting or drying events that may be large or infinitesimally small. As the column continues to desiccate, the single wetness value in Z-space continues to decrease. One possible representation of this sequence, in the Bins paradigm, or B-space, is shown in the right-hand column. In this case, wetness is not represented as a single value along a continuous spectrum from zero (dry) to one (wet), but as a combination of bins or buckets with constant wetness values, and varying relative area. During the drying sequence (moving top to bottom), area moves from wet bins to drier bins. It is important to keep in mind that actual water is *not* being relocated within the grid cell during this process, but *area* is.

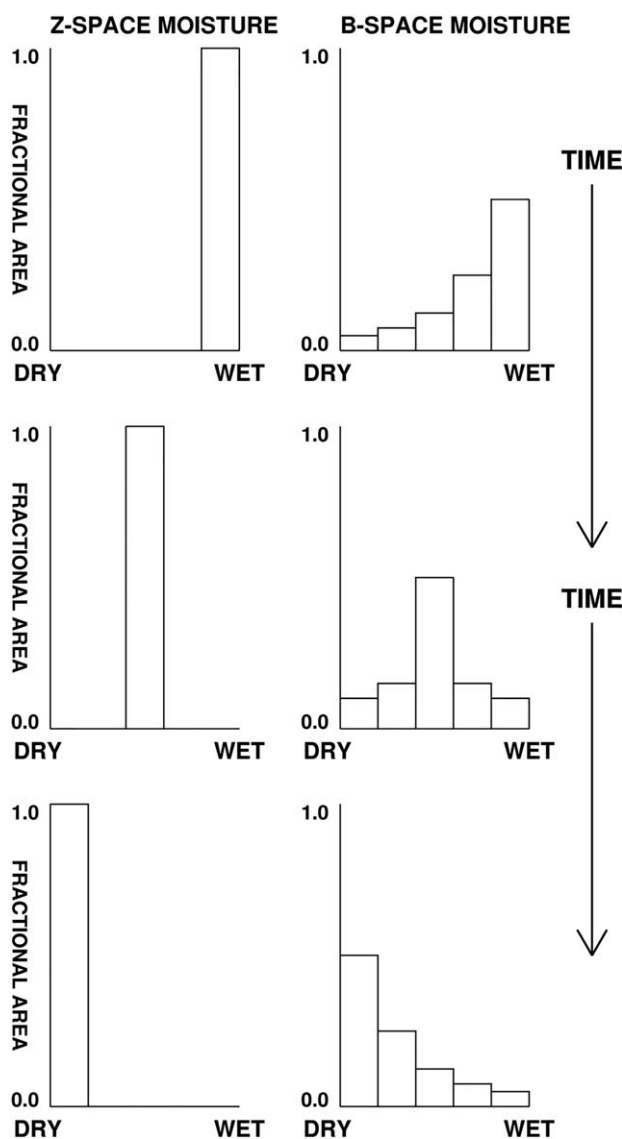


Figure 2. Conceptual diagram showing evolution of grid cell-mean vertically integrated soil moisture (left column) and soil moisture as determined using wetness bins (right column). See text for further explanation.

The relative wetness bin distribution shown here is only an example. During the drying process that can only be described in Z-space by the continuous movement of column wetness to the left (or to the right during moistening), the distribution of bin area is consistent with this wetness value. However, there is no restriction on the number of possible combinations of wetness bin areas that can describe a single column-mean wetness value. The bin distribution is an *emergent property* of the physical mechanisms (ET, runoff) that combine with meteorological forcing to drive the model.

In the simple model of SE07, soil wetness and evapotranspiration were calculated using a daily time step and single-layer soil. To incorporate this technique into the full SiB3 model requires reconciliation between the idea of vertically varying wetness, as represented by a layered soil model, and horizontally varying wetness, as represented by the Bins scheme.

In general, we use the Bins domain (B-space) to calculate horizontal water transfers (surface runoff), subsurface drainage out of the bottom of the soil, area-averaged controls on evapotranspiration, $\langle f(W) \rangle$ and the soil surface resistance to evaporation, $\langle R_{soil} \rangle$. It is important to note the distinction between a term obtained using multiple wetness bins, $\langle f(W) \rangle$, and one determined using a single area-averaged value, $f(\langle W \rangle)$. The B-space calculations also track and update the changes in the horizontal spatial variability of soil moisture due to precipitation, ET and runoff (surface and subsurface) by adjusting the fractional areas of the wetness bins.

The vertical domain, Z-space, is used to calculate the area-averaged vertical flows of water in the soil (infiltration, percolation); radiation; heat fluxes (latent, sensible, and ground) and exchanges of trace gases such as CO₂. Note that Z-space is used to calculate the surface-atmosphere fluxes as grid-area averages.

In short, we use each scheme to do what it does best: horizontal runoff due to both infiltration-excess and precipitation onto saturated areas and the effects of spatial variability are captured in B-space, while the area-averaged vertical transfers of mass and energy between the land and the atmosphere, and also vertical exchanges in the soil, are described in Z-space. Historically, the Z-space transfers are calculated only once per grid area per time step. The incorporation of B-space into SiB3 adds a negligible computational burden.

The distribution of area between moisture bins and the vertical distribution of water in soil layers are calculated independently; neither distribution is decomposed from the other. Self-consistency between B-space and Z-space is maintained through simultaneous calculations of processes affecting both B-space and Z-space at critical points in the calculation timeline (see next section).

We use the designation W (fraction of saturation) and bin increment $i = 1$ to $nbins$ (where $nbins = 10$, the number of soil wetness bins in the interval from 0 to 1) when referring to B-space. In Z-space, we describe volumetric water content ($m^3 H_2O m^{-3} soil$) as θ , and soil porosity, or maximum volumetric water content as θ_{sat} . Z-space soil depth is labeled as $j = 1$ to $nsoil$ (where $nsoil$ is the number of vertical soil layers, also 10) when referring to Z-space. Relative root fraction (*rootf*) in each Z-space soil layer follows Jackson *et al.* [1996], and soil physics generally follows CoLM [Dai *et al.*, 2003] and CLM [Lawrence *et al.*, 2011].

At all times, the total integral of water in the grid cell is balanced between Z-space and B-space, and mass is conserved:

$$\sum_{i=1}^{nbins} W_i a_i = \langle W_{tot} \rangle = \sum_{j=1}^{nsoil} \frac{\theta_j}{\theta_{sat}} \times \frac{\Delta z_j}{z_{tot}} \quad (3)$$

where a_i is the fractional area of each bin, θ_j and θ_{sat} are the layer-specific water content and porosity, respectively, Δz_j is the layer thickness, and z_{tot} is the total soil column depth. The term $\langle W_{tot} \rangle$ represents the grid cell-mean total-column soil wetness fraction. The discretization of equation (2), $f(W)$, into 10 wetness bins for the BR-PEG and US-ARM sites, is shown in Figure 1, plot b. $f(W)$ is constrained to have a value of zero at wilt point, and 1.0 (or no stress imposed) at field capacity. The exact location of wilt point and field capacity along the saturation gradient depends on soil character.

2.3. Order of Operations

In SiB3, soil moisture is predicted in a single operation, whereby infiltration, percolation, and water removal from the soil by roots and runoff are applied simultaneously to determine soil moisture content in individual soil layers. In the application of the Bins methodology, we have split these processes into separate steps, as shown in Figure 3. There are three steps at which B-space and Z-space must be considered

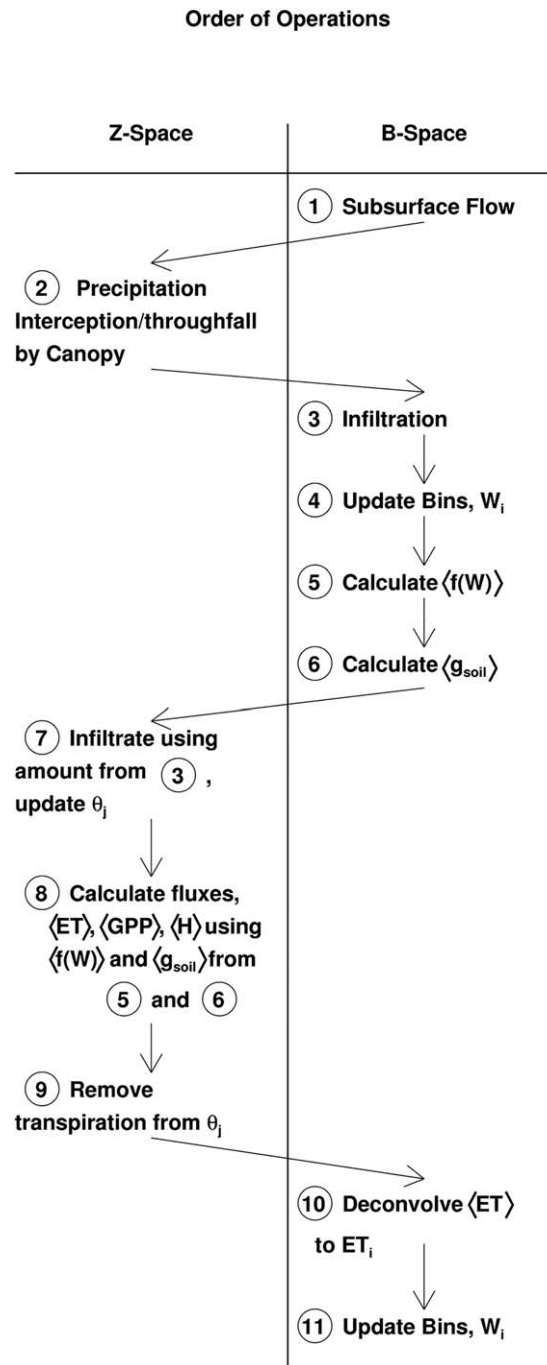


Figure 3. Order-of-operations schematic showing how code controlling individual processes and mechanisms is partitioned between the Z-space and B-spaces in SiB3-Bins.

fractional area of bin i for the grid cell. This approach is analogous to traditional treatments of drainage from the deepest soil layer in Z-space. The subsurface component of the water budget in B-space is calculated as

$$\delta W_{total}^{subscf} = \sum_{i=1}^{n_{bins}} -wout_i \quad (6)$$

which represents total subsurface drainage across the grid cell in units of fractional saturation of the total column. Once the subsurface drainage of water from bins has been calculated, the integrated subsurface

simultaneously to maintain water balance: The first is in the calculation of subsurface drainage (Step 1), where the lowest soil layer in Z-space must contain sufficient moisture to satisfy drainage requirements calculated in B-space. The second is in the calculation of infiltration (Step 3), where available pore space in the surface Z-layer must be large enough to accept water infiltrating from precipitation and/or interception storage. The third is in the calculation of soil surface evaporation (Step 8) where Z-space surface soil wetness, relative to the mean wetness in the Z-column, exerts influence on the amount of evaporation as calculated using relative area in the bins.

Step 1 is the calculation of subsurface runoff. We have applied a fractional area versus drainage relationship, where subsurface drainage is determined by wetness fraction. Moisture conductivity out of the bottom of each wetness bin is calculated as in Campbell [1974] or Clapp and Hornberger [1978] as

$$k_i = k_{sat} W_i^{2b+3} \quad (4)$$

where k_{sat} is saturated hydraulic conductivity (in $m s^{-1}$), b is an exponent that is dependent upon soil character, and i signifies wetness bin. To maintain consistency between Z-space and B-space we scale W_i in equation (4) by the ratio of the saturation fraction of the lowest layer in Z-space to the wetness of the Z-column as a whole. If the deepest Z-layers are relatively dry, then subsurface drainage will be reduced, regardless of wetness bin. We then calculate subsurface moisture drainage from each bin (with the exception of the driest bin, which is assumed to have no subsurface outflow) as

$$wout_i = \frac{k_i \Delta t}{\theta_{sat} z_{tot}} \times a_i \quad (5)$$

where subsurface runoff from each bin is assumed to leave the grid cell. The term Δt is time step, $\theta_{sat} z_{tot}$ represents the total pore space (in m) available to be filled with water over the vertical soil column, $wout_i$ has units of column-total fractional wetness, and a_i is fractional area of bin i for the grid cell.

flow leaving B-space (δW_{total}^{subsc}) is also removed from the deepest soil layer (θ_{nsoil}) in Z-space as total column subsurface runoff.

In Step 2 (Figure 3), rainfall (assumed to be spatially uniform in this study) is partitioned into a fraction that intercepts the canopy and a fraction that passes directly through the canopy, in Z-space. Rainfall intercepted by vegetation accumulates on leaves to a certain depth (dependent upon LAI), before running off leaves and onto the ground. Next, in Step 3 (B-space), water accumulates on the ground to a maximum depth of 1 mm. Puddle depth above this value is removed from the grid cell as overland runoff. Water is removed from this surface storage pool via infiltration and overland flow generated by any excess:

$$In\ fil_i = MIN\{(1 - W_i)a_i\theta_{sat}z_1\rho_{H_2O}, precipitation\} \quad (7)$$

where W_i is the fractional saturation of each bin, a_i is the fractional area of bin i , z_1 is the top soil layer thickness (in Z-space, the layer that the water will be infiltrating into), and ρ_{H_2O} is the density of water. The term $\theta_{sat}z_1\rho_{H_2O}$ represents the maximum amount of water that can be held in Z-layer 1, and we use θ_{sat} instead of θ_1 because Z-layer 1 is quite thin and water percolates quickly through it. Therefore, $In\ fil_i$ is the minimum of precipitation or the available pore space in layer 1 that can receive water, for each bin. Drier bins have more pore space available. Rainfall falling on the wettest bin is immediately converted into overland flow, and very heavy rainfall falling on subsaturated bins can also exceed the available pore space and generate infiltration-excess (Horton) runoff. The infiltration step requires coordination between B-space and Z-space as shown by the combination of z_1 and W_i in Equation (7). $In\ fil_i$ has units of meters of water per square meter of land, and is converted to a wetness fraction as follows:

$$\delta W_i^{in\ fil} = \frac{In\ fil_i}{\theta_s z_{tot}} \quad (8)$$

We now have two terms that describe the movement of water related to wetness bins; one associated with removal via subsurface runoff, and one representing infiltration of rainfall (if present). Each wetness bin will have a change in water content, given by

$$\delta W_i^{total} = \delta W_i^{in\ fil} - \delta W_i^{subsc} \quad (9)$$

With total change in water for each bin due to subsurface drainage and infiltration (δW_i^{total}) calculated, we now update relative bin area for the first time. Following SE07, a temporary bin-area array b_k , $k=1, nbins$ is created with zero area in each bin. Bin values W_k are identical to the original bin values W_i . For each $i=1, nbins$, we determine the index of the bin values on either side of the new interim moisture value ($W_i + \delta W_i^{total}$) as

$$W_k \leq W_i + \delta W_i^{total} \leq W_{k+1} \quad (10)$$

and a new area distribution is incremented for each b_k during the loop as

$$b_k = b_k + (1 - H)a_i \quad (11)$$

and

$$b_{k+1} = b_{k+1} + Ha_i \quad (12)$$

where

$$H = \frac{(W_i + \delta W_i^{total}) - W_k}{W_{k+1} - W_k} \quad (13)$$

Equations (11–13) must be looped over for all $k=1, nbins$ for each bin i (meaning 2 complete loops through the number of bins is required), and when completed the new area distribution b_k is copied back into the original area distribution a_i .

In Step 5, the area-averaged values of $\langle f(W) \rangle$ and $\langle R_{soil} \rangle$ are calculated by integrating these values at each bin midpoint multiplied by bin area as follows:

$$\langle f(W) \rangle = \sum_{i=1}^{nbins} f(W_i)a_i \quad (14)$$

where $f(W_i)$ represents the value of equation (2) for the wetness value in each bin. The term $\langle f(W) \rangle$ represents grid cell-integrated soil moisture influence on stomatal conductance, and therefore both transpiration and trace gas (e.g., CO₂) flux through stomates are regulated by this term.

In SiB, soil evaporation from the uppermost soil layer is regulated by a soil surface resistance term, R_{soil} [Sellers et al., 1995] (equation (3)). In SiB3-Bins, we use the inverse of R_{soil} to obtain a conductance term, g_{soil}

$$g_{soil} = \frac{1}{R_{soil}} = \left\{ \exp \left[d_1 + d_2 \left(\frac{\theta_1}{\theta_{sat} z_1 \rho_{H_2O}} \right) \right] \right\}^{-1} \quad (15)$$

where $\frac{\theta_1}{\theta_{sat} z_1 \rho_{H_2O}}$ is the surface layer soil wetness and d_1 and d_2 are empirical constants. In the Bins paradigm, we can replace the surface layer soil wetness term $\frac{\theta_1}{\theta_{sat} z_1 \rho_{H_2O}}$ with bin wetness values W_i . When calculating g_{soil} using wetness bins, we scale W_i by the ratio of surface wetness in Z-space to mean Z-column wetness to maintain consistency between Z-space and B-space. This scaling term inhibits soil surface evaporation when surface soils are dry, and increases it when the surface is moist such as immediately following precipitation events. In the calculations, we use an evaporation “conductance,” g_{soil} , to avoid numerical issues associated with large resistance to evaporation in dry soils.

In Step 6, we obtain a grid cell-mean value for $\langle g_{soil} \rangle$ from the wetness bin distribution as

$$\langle g_{soil} \rangle = \sum_{i=1}^{n_{bins}} (g_{soil})_i \times a_i \quad (16)$$

where $(g_{soil})_i$ represents the surface soil evaporation resistance for each wetness bin as determined by equation (15). Scaling the $\langle g_{soil} \rangle$ by relative wetness in the surface layer of Z-space also prevents artificial enhancement of evaporation conductance in soils with high clay content, where wilt point may occur at high relative wetness compared to sandy soils.

In Step 7 (Z-space), infiltration and percolation are now computed for the vertical soil layers following the Richards equation approximation to Darcy’s law prior to the surface flux calculation. The integrated resistance terms, $\langle f(W) \rangle$ and $\langle R_{soil} \rangle$ are ready to be applied to the full model calculations of energy and moisture fluxes, stomatal conductance, and photosynthesis. Surface exchanges of energy, moisture, momentum, and trace gases are then computed in Z-space (Step 8), as in the past, with a single set of calculations for the grid area.

Water is removed from the soil from direct evaporation (λE_{sfc} : soil layer 1 only) and transpiration (λE_T : every soil layer containing roots) in Step 9. These ET components are regulated by the values of $\langle f(W) \rangle$ and $\langle g_{soil} \rangle$ computed previously. This is done by setting

$$\theta_1 = \theta_1 - \lambda E_{sfc} - \lambda E_T \text{root}f_1 \quad (17)$$

for the top soil layer, and

$$\theta_j = \theta_j - \lambda E_T \text{root}f_j \quad (18)$$

for soil layers $j = 2$ to n_{soil} where $\text{root}f_j$ is relative root fraction.

Finally, in Step 10, the area-averaged losses and gains of moisture and CO₂ from Step 8 are deconvolved using equations (10)–(13) to allow updating of the fractional areas associated with each bin. We maintain consistency with the grid-average moisture fluxes (soil surface evaporation and transpiration) in each bin i by requiring that

$$\delta W_i = \lambda E_{sfc} \frac{(R_{soil})_i}{\langle R_{soil} \rangle} + \lambda E_T \frac{f(W_i)}{\langle f(W) \rangle} \quad (19)$$

It follows that total water removal from the soil by transpiration and surface soil evaporation, as represented in the bins, is

$$\delta W_{tot} = \sum_{i=1}^{n_{bins}} \delta W_i = \lambda E_{sfc} + \lambda E_T \quad (20)$$

This numerical scheme maintains consistency between the wetness bins (B-space) that represent an abstraction of moisture distribution across the landscape, and the explicit representation of the vertical

distribution of water in individual soil layers (Z-space). The vertical soil water distribution represents an integration of the probability density function of bin areas, and does not maintain fidelity to any individual wetness bin. A wetter soil will manifest as an overall increase in wetness across vertical soil layers as well as a movement of area into bins of higher wetness. As soils dry out the grid cell-mean wetness as represented in the vertical soil layers will decrease, and area will be transferred from wet to drier bins. Just as there is no single distribution of bin area that corresponds to a single grid cell-mean or column-mean wetness value, there is no single vertical distribution of water that corresponds to a single mean wetness. A soil with relatively wet surface layers in Z-space (corresponding to a wetting front, perhaps), or a soil with dry surface and wetness at depth (as a result of prolonged ET with little or no precipitation) can have identical column-mean wetness values. The variability in Z-space and B-space, while maintaining consistency and water balance, is another emergent property of the Bins paradigm.

3. Results

With the conceptual model of SE07 installed into SiB3, we now turn to comparing simulations made using the Bins method of determining soil moisture stress on ET with control runs. In the control runs, we use a grid cell-mean soil wetness value to obtain $f(\langle W \rangle)$, and the Bins value is calculated using the bin-level values of $f(W)$ normalized to the density function of bin area to obtain $\langle f(W) \rangle$. Both simulations use the formulation of $f(W)$ given in equation (2). In selecting test sites, we chose sites that are expected to occupy the steepest nonlinear part of $f(W)$ for at least a part of the year, preferentially over extremely wet or dry locations that may not traverse the extremely steep portion of the $f(W)$ curve during the annual cycle.

We simulate regions where soil moisture is a significant control on ecosystem behavior, so initial conditions are critical. Rather than initialize a model “cold start” (for both control and Bins runs), we “spin-up” all simulations by running multiple cycles of the available meteorology. For both the Bins and control runs, the initial bin area distribution is irrelevant if enough years are simulated (>20). For all runs, we initialize with uniform soil temperature set at the annual mean air temperature, and all Z-layers set to 95% of saturation, which corresponds to all area in the wettest bin. Control and Bins simulations are run identical number of years for spin-up.

For evaluation, we compare model fluxes to observed fluxes from eddy covariance towers. This is not an optimal comparison, as the Bins paradigm is designed to address behavior on scales larger than a flux tower footprint. However, flux tower data offer the possibility for straightforward evaluation of model behavior across multiple ecosystems. Since the focus of this paper is to determine how the Bins method translates from an idealized application into a fully resolved land model, we believe flux data are a reasonable method for evaluation. Bins behavior across larger scales will be the focus of subsequent research.

3.1. Pe de Gigante, BR-PEG

Pe de Gigante is a woodland savanna (*cerrado sensu strictu*) site in São Paulo state, Brazil [da Rocha et al., 2002]. Annual precipitation is ~ 1300 mm yr^{-1} , with a wet season during Austral summer and a dry season (precipitation < 100 mm month^{-1}) [Goulden et al., 2004] of 7 months or more. At 21.6° South latitude, the BR-PEG site has some seasonality in annual temperature ($\sim 5^\circ\text{C}$ amplitude in monthly mean temperature) and radiation, but the site does not experience a traditional “winter” with dormant vegetation (Figure 4, plot a). The site is water-limited in that soil moisture is a strong regulator of surface flux (i.e., “vegetation control” over ET) [da Rocha et al., 2009; Costa et al., 2010], as the evaporative fraction ($\lambda E / (H + \lambda E)$) is large in the wet season (which is a sink of CO_2) and small in the dry season (source of CO_2). We simulate the years 2001–2003 [DeGonçalves et al., 2013] inclusive, and evaluate simulated fluxes of heat, moisture, and CO_2 against observations from the LBA-MIP effort [DeGonçalves et al., 2013; Baker et al., 2013]. Observations of latent and sensible energy fluxes are available for 2001–2002 [DeGonçalves et al., 2013], and carbon fluxes at this site are obtained from Restrepo-Coupe et al. [2013] and are available for 2002–2003. Baker et al. [2013] demonstrated an ability to reproduce observed fluxes using SiB3, but in that case the treatment of $f(W)$ was modified with an *ad hoc* landscape-scale relaxation following Baker et al. [2008]. In the current simulations, we apply the strict treatment of $f(\langle W \rangle)$ in the control runs as described above.

Meteorological drivers (pressure, temperature, precipitation) are obtained from instruments on the tower [DeGonçalves et al., 2013], and vegetation phenology (LAI, fraction of Photosynthetically Active Radiation,

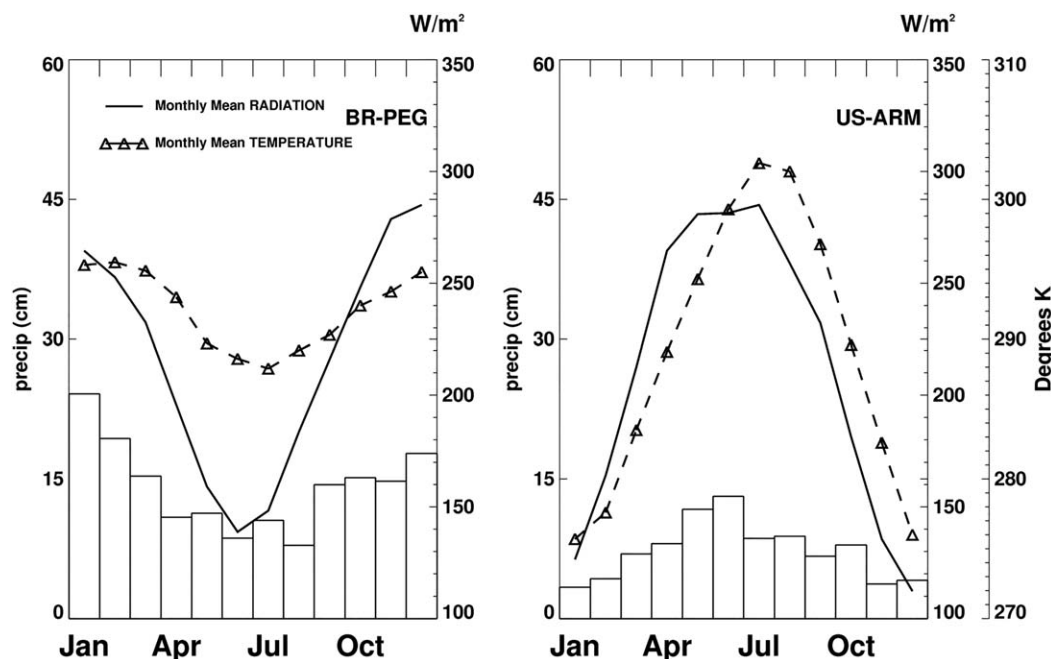


Figure 4. Mean annual cycle of precipitation, radiation, and temperature for the (a) BR-PEG and (b) US-ARM tower sites.

fPAR) are obtained from the MODIS collection 5 Global Land Cover Subsetting tool [ORNL DAAC, 2008a, 2008b]. The model is spun up for 21 years, or seven cycles over the 3 years of available forcing data.

Monthly averaged fluxes of CO₂, water, and energy (Figure 5) can clearly be seen to improve in the Bins simulation when compared to the control. Carbon flux shows extreme variability in the control run at times switching from source to sink or back from month to month. The control run demonstrates a rapid transition from CO₂ sink to source following the end of the wet season, in disagreement with observations and the Bins simulation. Dry season control run LE is small compared to observations, suggesting an oversensitivity to water stress in the soil. Sensible heat flux (H) is overestimated in both simulations, but the excess is larger in the control run. The Bins simulations show much more fidelity to observations than the control. Statistical evaluation at BR-PEG was performed, but are not significant due to the small number of data points (24 monthly values, but each month is not necessarily independent), and therefore are not presented.

The bins-weighted and area-mean calculations of $f(W)$ are shown in plot d of Figure 5, along with the values of mean soil wetness (W) for the Bins and control runs. W is not identical between the two runs because ET and infiltration vary based on model formulation. In the control run, $f(W)$ shows large variability in response to small changes in total soil wetness, while $f(W)$ in the Bins runs evolves in a smoother manner.

The distribution of relative area in the 10 wetness bins, shown as a snapshot taken at the end of each month in 2003, is shown in Figure 6. LAI is relatively invariant during the year at values between 2 and 3 (not shown) and temperatures are above freezing in all months, meaning that transpiration will be attempting to draw moisture out of the soil during the entire year. Overall ET is partitioned more toward transpiration (~80%) in both SiB3-control and SiB3-Bins simulations due to the combination of persistent shading by the canopy and the high sand content, which allows rapid percolation of water downward resulting in dry surface soils. As soils dry during seasonal drought stomates close and evaporative fraction decreases to values of 0.5 or less. BR-PEG was relatively wet at the close of calendar year 2002, so at the end of January (Figure 6, plot a) area is accumulated in wetter bins on the right of the distribution, with a peak in bin 7. February and March 2003, while wet, did not have as much precipitation. Area is still accumulated in wetter bins, but the peak in these months is in bin 6. As the system dries further from April to June (plot b), the peak wetness moves further left to bin 5, and in June area begins rapidly accumulating in drier bins, with a hint of bimodality in bin 2. July and August are distinctly bimodal with peaks in bins 2 and 4, and by

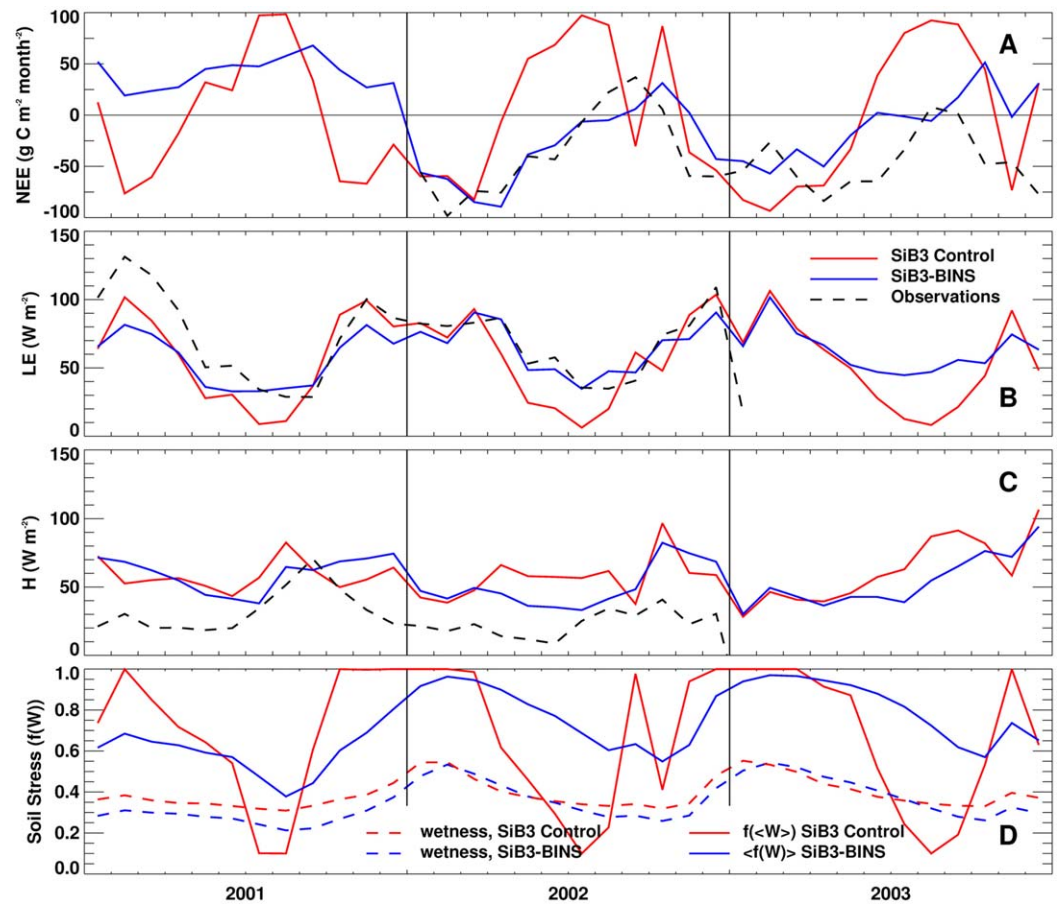


Figure 5. Monthly averaged values of (a) net carbon exchange (NEE), (b) latent heat (LE), (c) sensible heat (H), and (d) soil stress function/mean wetness of soil column for SiB3 control (red) and SiB3-Bins (blue) simulations at BR-PEG for years 2001–2003.

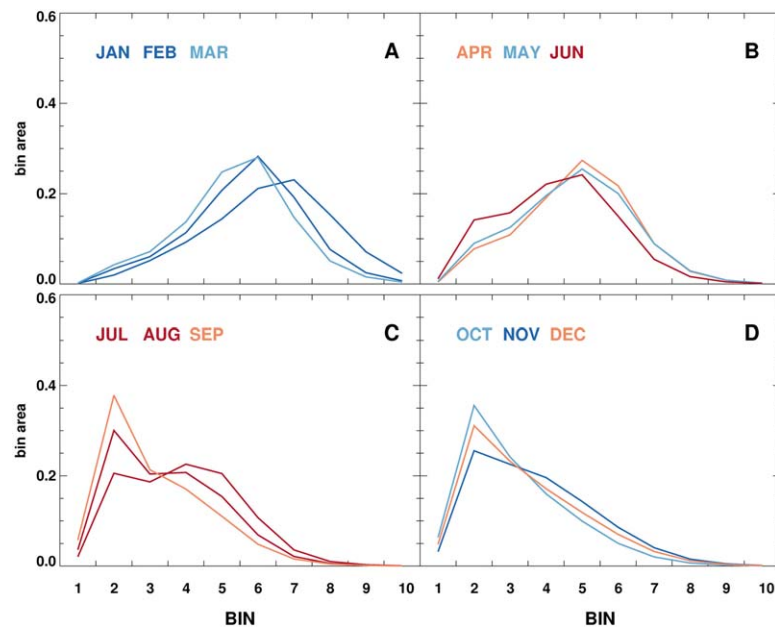


Figure 6. Distribution of area for soil wetness bins 1–10 for year 2003 at BR-PEG as simulated by SiB3-Bins. Bin distribution is plotted for the last day of each month. Line colors are coded to precipitation amount; the three wettest months (January, February, November) are shown in dark blue, the driest months (June, July, August) are deep red, and intermediate months are lighter shades of each.

September the secondary peak in bin 4 is gone. During October and November, the peak area remains in bin 2 even though November was the second wettest month of the year, and the amount of area in bin 2 decreases as area is added to wetter bins. December is anomalously dry, so the distribution moves left toward drier bins again during the month. Since $f(W) = 0$ in bin 2 results in stomatal closure, area can only be accrued into bin 1 by evaporation from the soil surface. This can be seen to happen in July to September (plot c). Theoretically, extremely strong ET could force area into bin 1 past the stomatal closure of bin 2 (Figure 1), but in these simulations ET is constrained when area is in bin 2 to the extent that accumulation of area in bin 1 is minimal. When the grid cell is wet, area is maximized in bins where $f(W) = 1$ (bin > 3), and stomates are open. This behavior is consistent with the idea of “environmental control” over ET as described by *Costa et al.* [2010] and *da Rocha et al.* [2009]. Spatial variability, as represented in the bin area distribution, is much smaller during the driest months (when significant area is in bin 2 only) than in the wet season, when area is spread over many wetness bins. We find that spatial variability in soil wetness (as represented by bin area distribution) is greater during wet periods and decreases with overall desiccation, consistent with the findings of SE07.

3.2. Southern Great Plains, US-ARM

We simulate 7 years (2000–2006) at the winter wheat crop site at the Atmospheric Radiation Measurement Southern Great Plains Central Facility (US-ARM) [*Fischer et al.*, 2007; *Raz-Yaseef et al.*, 2015]. We simulate this site at a grassland in SiB3. This site is more seasonal than BR-PEG, residing at 36.6° North latitude (Figure 4, plot b). Mean annual precipitation is $\sim 900 \text{ mm yr}^{-1}$, with maximum during Boreal summer. LAI and fPAR are seasonal, and the site is dormant during the winter. Driver meteorology and observed flux data are taken from data sets provided by the North American Carbon Project (NACP) Site-Synthesis experiment [*Schwalm et al.*, 2010]. Precipitation data in the NACP files exceeded climatological expectation, so we scaled precipitation amounts to align them with Global Precipitation Climatology Project (GPCP) [*Adler et al.*, 2003] following the method of *Baker et al.* [2010]. Phenology (LAI, fPAR) were again taken from MODIS land cover subsets [*ORNL DAAC*, 2008a, 2008b]. As with BR-PEG, we initialized SiB-Bins with a saturated, isothermal soil, and spun up the model over multiple cycles of the 7 year data record.

The improvement in model performance is not as dramatic at US-ARM as at BR-PEG (Figure 7). Both models match the timing, but fail to simulate the strong uptake of CO_2 observed in April. This may be related to the respiration parameterization used in both models that follows *Denning et al.* [1996], which results in a balanced carbon budget, as opposed to the net sink shown in the observational data. Seasonal cycles of latent heat are better in the Bins simulations in 2004 and 2005, but the control is superior in 2003 and both models underestimate late-summer LE in 2006. Sensible heat from the Bins simulation is worse than the control in 2003, Bins is a clear improvement in 2004, both models exceed observations in 2005, and both models are reasonable in 2006. Statistically, the Bins simulations explain a larger fraction of observed variability (Table 1; significant to 99%) for both LE and H, but not for NEE. Bins normalized error, where a smaller value represents a better comparison, is smaller for LE, slightly larger for H, and similar to control for carbon flux. Overall, our fidelity to observations is favorable when compared to previous studies [e.g., *Liu et al.*, 2013; *Schwalm et al.*, 2010]. Our simulations are consistent with *Schwalm et al.* [2010], who found that grasslands and crops were more poorly simulated than forests when compared across a suite of LSPs.

Similar to BR-PEG, the control wetness function $f(\langle W \rangle)$ displays extreme variability in response to small changes in mean soil wetness, as the wetness $\langle W \rangle$ resides on the steep part of the curve for much of the simulation period (Figure 7, plot d). The Bins soil wetness function $\langle f(W) \rangle$ behaves smoothly.

In the control run, there was a general tendency for overestimation of latent heat at all times, but especially during the summer months. LAI has peak value around 2, so potential transpiration is not large. We found that soil evaporation in the control runs was approximately 80% of overall ET, which sometimes exceeded observed ET by 30–40 W in the monthly average (Figure 8). In the Bins simulation, soil surface evaporation was considerably reduced to the point where evaporation from soil is generally less than transpiration in the monthly mean. This low surface evaporation was persistent even when $\langle f(W) \rangle$ was larger in the Bins run than in the control. This is due to coupling bin-determined soil surface evaporation to the surface layer wetness in Z-space. Once this surface Z-layer becomes dry, soil surface evaporation is suppressed regardless of the value of $\langle f(W) \rangle$. We believe that the partitioning and overall value of latent heat in the Bins formulation is more realistic.

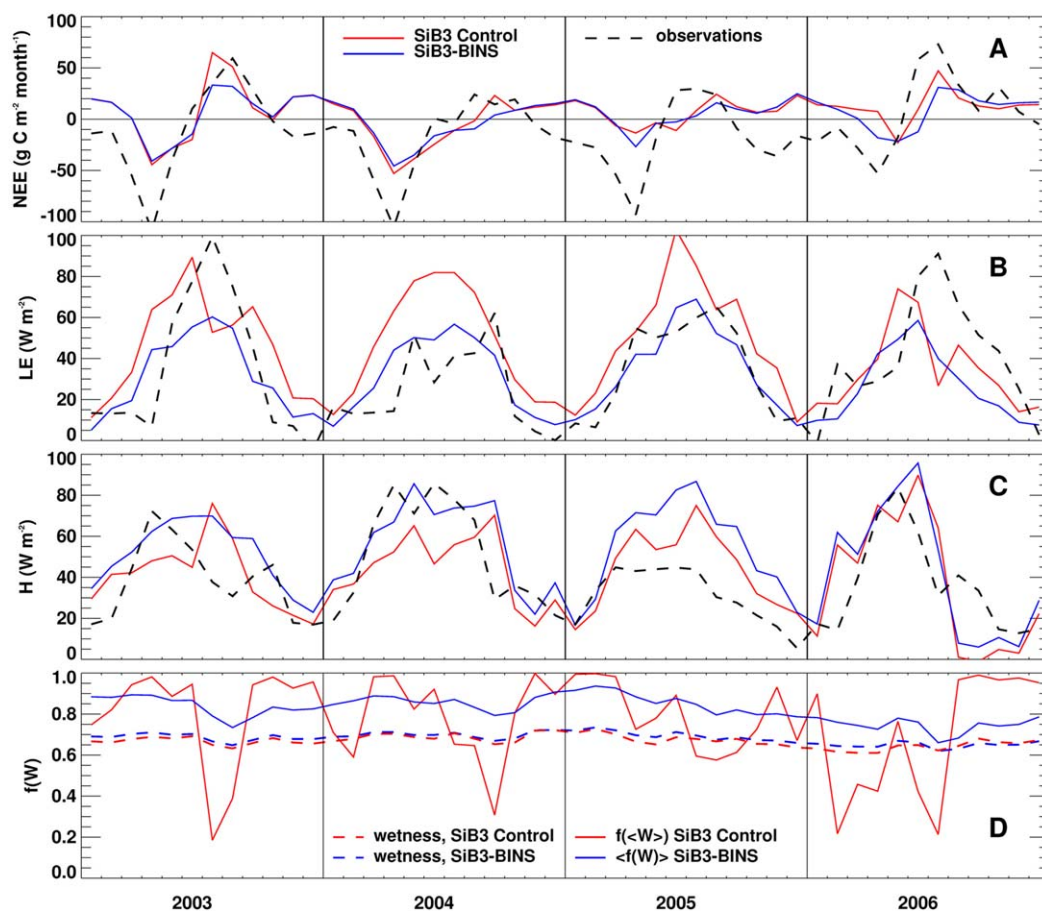


Figure 7. Monthly averaged values of (a) net carbon exchange (NEE), (b) latent heat (LE), (c) sensible heat (H), and (d) soil stress function/mean wetness of soil column for SiB3 control (red) and SiB3-Bins (blue) simulations at US-ARM) for years 2003–2006.

The evolution of area in wetness bins over a single year (2001) at US-ARM is shown in Figure 9. Bin area has reduced dynamic range and is concentrated in wetter bins when compared to BR-PEG, largely due to the higher clay content at US-ARM, which moves wilt point and field capacity to higher relative wetness (Figure 1). We find that there is not a concentration of area in the bins near wilt point (bins 5 and 6) during the dry season, as there was at BR-PEG. This is likely due to the fact that the dry season at US-ARM is winter, when LAI/fPAR are low, and temperatures are too cold for photosynthesis. Evaporation from surface soil can also be suppressed by either frozen soil or snow. In January and February 2005, area was concentrated in bin 8 due to wet fall months in 2004, but the peak moved to bin 7 in March due to both lack of precipitation and increasing ET in spring. In the latter part of the year (Figure 9, plots b–d), area oscillated between maxima in bins 7 or 8 in response to precipitation and ET, and settled into bin 7 in response to dry months at the end of the year.

Table 1. Simple Statistics for US-ARM^a

STAT	US-ARM					
	LE		H		NEE	
	CTRL	BINS	CTRL	BINS	CTRL	BINS
R^2	0.33	0.54	0.30	0.45	0.42	0.24
NSEE	0.61	0.42	0.46	0.49	0.84	0.84

^aShown are the fraction of variability in observations explained by each model, as well as the normalized standard error of the estimate, for SiB3-control (CTRL) and SiB3-Bins (BINS) simulations. NSEE is calculated as the root mean square deviation between model and observations divided by the root mean square of the observations.

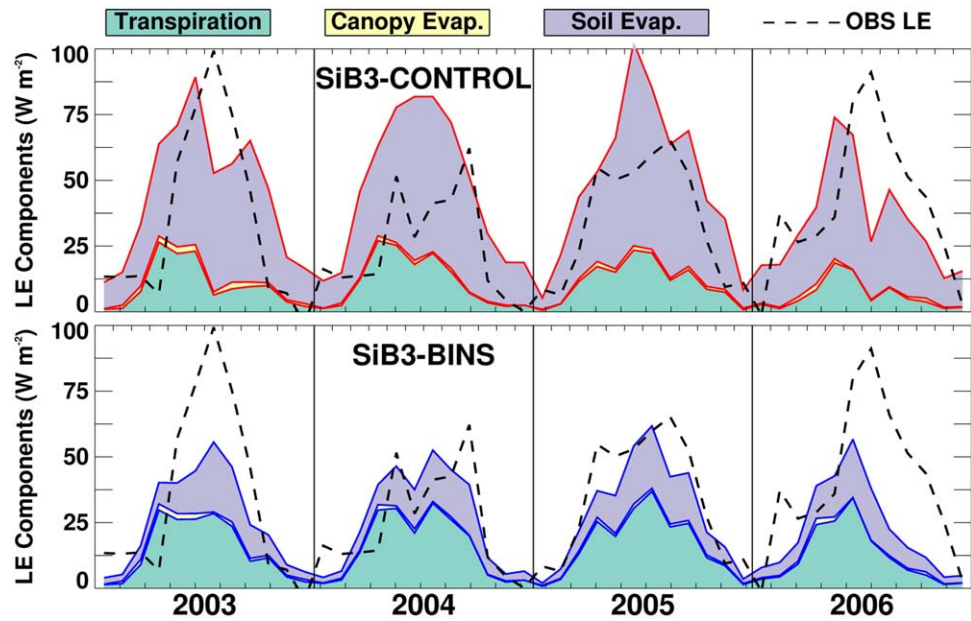


Figure 8. Partition of monthly mean total latent heat flux into transpiration, evaporation of water off canopy, and soil surface evaporation. Evaporation of surface interception stores (puddles) is minimal. SiB3-control is shown in top plot, SiB3-Bins in the bottom plot.

Curiously, the value of $f(W)$ at US-ARM is consistently high, suggesting little or no restriction of plant behavior by soil moisture. This is due to the vegetation at US-ARM, which has a maximum LAI of $1.5-2 \text{ m}^2 \text{ m}^{-2}$ for a brief period in spring in the MODIS retrieval. There is not enough leaf area to draw water out of the soil, even when there is little or no stress on transpiration. The surface soil becomes desiccated relative to the rest of the soil column, which has the effect in the Bins simulation of increasing resistance to soil surface evaporation. In this manner, the evaporative fraction is lower compared to the control run, and variability corresponds more closely to observations (Figure 7).

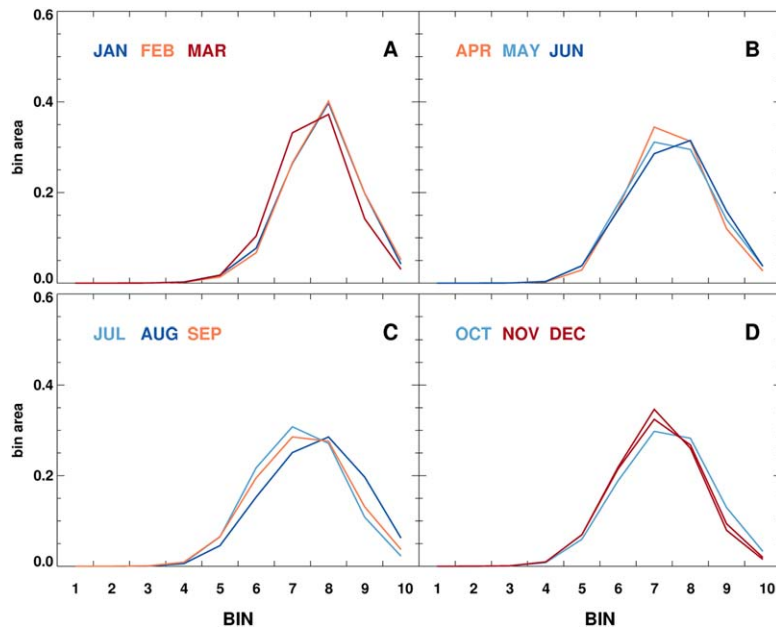


Figure 9. Distribution of area for soil wetness bins 1–10 for year 2005 at US-ARM as simulated by SiB3-Bins. Bin distribution is plotted for the last day of each month. Line colors are coded to precipitation amount; the three wettest months (January, February, November) are shown in dark blue, the driest months (June, July, August) are deep red, and intermediate months are lighter shades of each.

4. Discussion

In simulations at two distinctly different semiarid sites, we found that surface behavior was reproduced when simulated using the Bins formulation compared with a control. The behavior was distinctly different at tropical site BR-PEG where photosynthesis and transpirational removal of water from soil occurred throughout the year, as opposed to US-ARM where ecosystem activity was dormant in winter. We found this difference in seasonality resulted in significant changes in the evolution of bin area through the year, above what was expected due to dissimilarities in clay and sand content in the soil. This demonstrates that the Bins scheme is suited to simulate ecosystems across a range of variability in climate space.

The representation of moisture stress on transpiration is significantly different between the control and Bins simulations. Figure 10 shows a period of drying and moistening at BR-PEG in 2001. From 12 May (after the wet season has ended yet soils are still moist) to 12 September, there is little or no precipitation and soil moisture decreases with attendant decrease in stress function value $f(W)$ (Figure 10, plot a), whether determined by the area-mean value in the control simulation or by bin area distribution. The red curve shows the control run, and this curve follows the very nonlinear form of equation (2) and Figure 1. The Bins behavior is much different. At the beginning of the drying period (blue curve in plot a), $\langle f(W) \rangle$ is significantly smaller than $f(\langle W \rangle)$, due to the existence of some area in bins where $f(W_i) < 1$. As the soil dries due to ET, the reduction in Bins wetness function is muted compared to the control run (red), due to the transfer of area from wetter to drier bins. It is only when root-weighted soil moisture approaches wilt point that the Bins $\langle f(W) \rangle$ begins to drop steeply. A period of moistening between 12 September and 31 December is also shown in Figure 10 in plots b and c. In the control moistening follows the same curve as drying but this

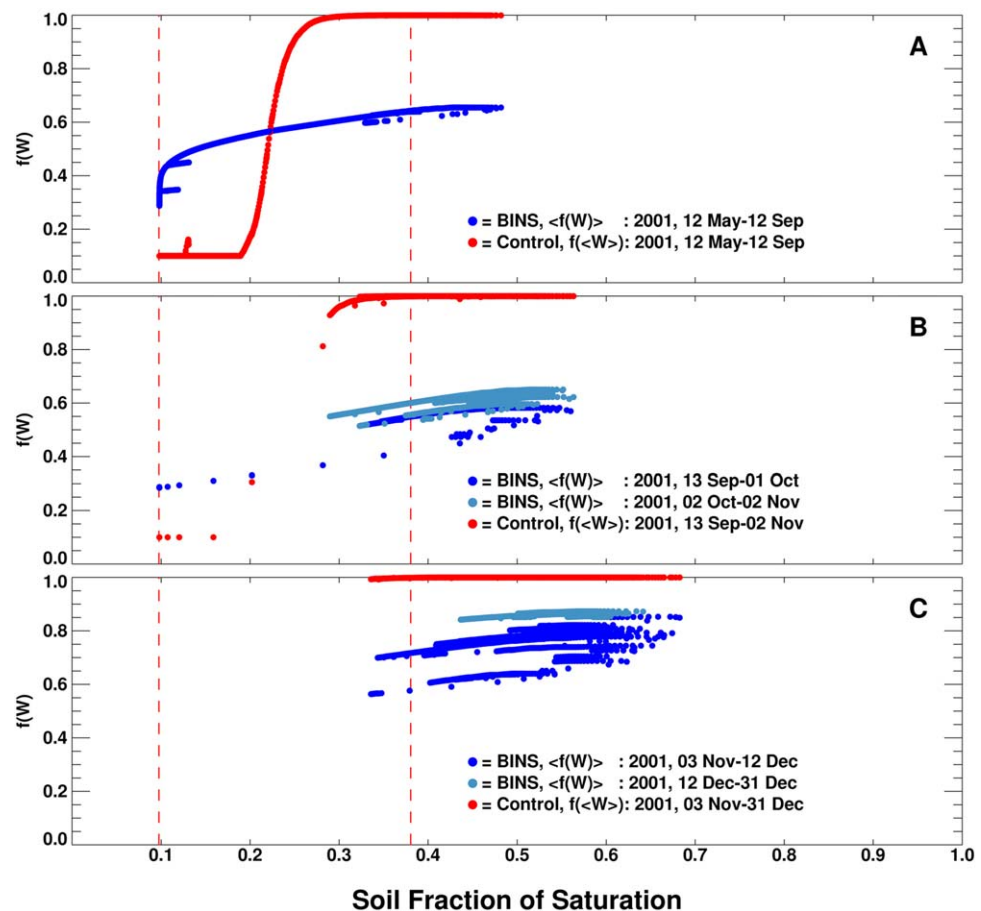


Figure 10. Soil moisture stress at BR-PEG as a function of root-weighted soil moisture for the SiB3 control run (red) and SiB3-Bins run (blue), for the period 12 May to 31 December 2001. (a) Drying period, 12 May to 12 September, when there is little or no rain. (b) Rapid moistening in the last 2 weeks of September. (c) Further moistening in November and December.

control curve can move slightly left or right in response to variability in the relationship between vertical moisture and root distributions. The form is essentially the same during both the drying and moistening periods and follows the nonlinear form of the equation. Furthermore, extremely small changes in total soil moisture can have drastic effects on the value of $f(\langle W \rangle)$, so that in the control simulation the ecosystem can shift from extreme stress to no stress at all in just an hour or two, which is unrealistic. Bins moistening and return of the stress function to values near 1 does not take place in a single rapid jump, but rather in response to individual precipitation events that occur stochastically. In Figure 10 (plots b and c), we color-code wetting events temporally, with darker-colored (blue) events happening earlier in the period of moistening (13 September to 31 December). The initial precipitation event (12–30 September, Figure 10, plot b) results in root-weighted column soil moisture content quickly rising, yet $\langle f(W) \rangle$ does not jump immediately, as the movement of area into wetter bins is temporally buffered when compared to the control run in that the incremental increase in soil moisture is reflected as small changes in bin area distribution and incremental rise in $\langle f(W) \rangle$. Ecosystem-scale stress is eased through moistening that takes place on the scale of days or weeks rather than hours. Through the end of the year, the overall trend is toward wetter soils, but this happens in a pattern of wetting events separated by intervals where the soil dries somewhat. Figure 10 shows that the overall soil wetness increases from 30% of saturation in mid-September to 50–60% saturated by the end of the year, but does so in a somewhat oscillatory fashion. Root-weighted soil wetness jumps up during precipitation events, and drops during drying intervals, all the while moving toward a general trend of increasing soil moisture. Superimposed on this trend is the behavior of $\langle f(W) \rangle$, which is slowly increasing as area is moved into wetter bins. This can also be seen in plot d of Figure 5, where the value of $f(\langle W \rangle)$ (red) jumps rapidly to 1.0 while the value of $\langle f(W) \rangle$ (blue) increases at a slower rate.

Vertical distribution of water can vary in the Bins simulations. It is possible to have multiple vertical distributions of water in Z-space for a single PDF of bin area. Similarly, a given vertical distribution of water in Z-space is not associated with a unique PDF of bin area. While water in Z-space and B-space is self-consistent and functionally linked, differences between Z-space soil water and the value of $\langle f(W) \rangle$ result in a subtle range of responses of soil surface evaporation and transpiration to precipitation events in SiB3-Bins that appear to be more realistic than the simulations generated by the control runs.

5. Conclusions and Further Research

The implementation of the Bins scheme of SE07 into a 1-D version of a modern LSP, SiB3-Bins, has been successfully accomplished with negligible additional computational burden. The reconciliation of the original vertically oriented SiB3 (Z-space) with the Bins scheme abstraction (B-space) was achieved relatively simply and balances water when compared between B-space and Z-space. We find that SiB3-Bins has improved simulation of the time-variation of evapotranspiration rates during drydown when compared to SiB3-control, mainly due to the smoothing effects of accounting for the effects of soil moisture spatial variability in the area-averaged $\langle f(W) \rangle$ and $\langle R_{soil} \rangle$ calculations. We also simulate smoother recovery of evapotranspiration rates when exiting from drydowns in SiB3-Bins. Note that entry into and recovery from drydowns give rise to apparent hysteresis in the area-averaged $\langle f(W) \rangle$ function. We believe this attenuated response is more realistic when compared to SiB3-control simulations that can switch from extreme stress to no stress in a matter of hours.

The focus of the research presented here was to determine whether the Bins method for representing spatial heterogeneity in soil wetness is viable when installed into a more complex land model as opposed to the extremely simple model of SE07. With that viability established, we can turn attention to expanding the research scope.

Performing global simulations of surface flux driving SiB3-Bins with reanalysis data are a natural next step. We will be able to evaluate behavior against other established models and study SiB3-Bins simulation of recent drought events such as those in Amazonia in 2005, 2010, and 2015, Russia in 2010, and the central USA in 2012.

In the present application, topography is not considered. There is no transfer of water from bin to bin, such as might happen when runoff from hillslopes (perhaps representing dry bins) collects in riparian areas (wet bins). SiB3-Bins is naturally extendable to use data such as topographic index to calculate between-bins surface and subsurface runoff. Currently both surface and subsurface runoff leave the grid cell. Allowing

between-bin flow from hilltop to riparian areas in a manner analogous to some of the statistical-dynamics approaches could enhance realism in SiB3-Bins.

The treatment of precipitation partition into stratiform and convective components has long been problematic in LSPs, and is neglected in many treatments of surface heterogeneity. Treatment of stratiform precipitation is simple, as this rain/snow can be expected to fall over the entire grid cell. Convective precipitation, on the other hand, is problematic for models to simulate. One option is to distribute rainfall from convective cells across the entire GCM grid cell. In this case, the convective precipitation will fall as light rain or mist, and frequently evaporates directly off leaves without ever reaching the soil and unrealistically enhances ET [Shuttleworth, 1988]. Alternatively, convective rain can be calculated to impact only a fraction of the vegetation, where buildup on leaves quickly exceeds storage capacity, runs off, and is available at the soil surface for runoff or infiltration. In the latter case, infiltrated rainwater is immediately present over the entire grid cell. The Bins paradigm offers a solution, in that convective rainfall can impact a fraction of each wetness bin. In this case, the high impact of heavy rain over a small area will be manifest as buffered changes in wetness bin distribution, and large excursions of grid cell-level behavior (or no impact, in the mist case) will not result.

We have demonstrated that SiB3-Bins is not limited to the simple application of SE07, and can in fact function when installed in a more complex model with explicit treatment of physical processes. SiB3-Bins performs similarly to a control simulation, and improves representation of some aspects of surface flux in experiments performed at two sites that experience water limitation within traditional modeling frameworks. The partitioning of area into a distribution of bins of varying wetness is an emergent property of model construction, and provides a novel new treatment of moisture heterogeneity on GCM-scale grids that exhibits promise for future research.

Acknowledgments

This research was sponsored by the NASA contracts NNX15AW96G and NNX14AI52G, Department of Energy contracts DE-SC0014438 and DE-SC0014426, as well as the National Science Foundation Science and Technology Center for Multi-Scale Modeling of Atmospheric Processes (CMMAP), managed by Colorado State University under cooperative agreement ATM-0425247. The authors thank CMMAP director D.A. Randall for his interest in this project and encouragement during the research process. Data used are listed in the references, model code and output are available from the corresponding author at ian.baker@colostate.edu upon request. Observations collected at the US Southern Great Plains site (US-ARM) were supported by the Office of Biological and Ecological Research of the US Department of Energy under contract no. DE-AC02-05ch11231 as part of the Atmospheric Radiation Measurement (ARM) Program. The authors also would like to acknowledge the anonymous reviewers whose contributions greatly improved the manuscript.

References

- Adler, R. F., et al. (2003), The Version 2 Global Precipitation Climatology Project (GPCP) monthly precipitation analysis (1979-present), *J. Hydrometeorol.*, *4*, 1147–1167.
- Arain, M. A., F. Yuan, and T. A. Black (2006), Soil-plant nitrogen cycling modulated carbon exchanges in a western temperate conifer forest in Canada, *Agric. For. Meteorol.*, *140*, 171–192, doi:10.1016/j.agrformet.2006.03.021.
- Avisar, R., and R. A. Pielke (1989), A parameterization of heterogeneous land surfaces for atmospheric numerical models and its impact on regional meteorology, *Mon. Weather Rev.*, *117*, 2113–2136.
- Baker, I. T., A. S. Denning, N. Hanan, L. Prihodko, P.-L. Vidale, K. Davis, and P. Bakwin (2003), Simulated and observed fluxes of sensible and latent heat and CO₂ at the WLEF-TV Tower using SiB2.5, *Global Change Biol.*, *9*, 1262–1277.
- Baker, I. T., L. Prihodko, A. S. Denning, M. Goulden, S. Miller, and H. da Rocha (2008), Seasonal drought stress in the Amazon: Reconciling models and observations, *J. Geophys. Res.*, *113*, G00B01, doi:10.1029/2007JG000644.
- Baker, I. T., A. S. Denning, and R. Stöckli (2010), North American gross primary productivity: Regional characterization and interannual variability, *Tellus, Ser. B*, *62*, 533–549, doi:10.1111/j.1600-0889.2010.00492.x.
- Baker, I. T., et al. (2013), Surface ecophysiological behavior across vegetation and moisture gradients in Amazonia, *Agric. For. Meteorol.*, *182–183*, 177–188, doi:10.1016/j.agrformet.2012.11.015.
- Ball, J. T., I. E. Woodrow, and J. A. Berry (1987), A model predicting stomatal conductance and its contribution to the control of photosynthesis under different environmental conditions, in *Progress in Photosynthesis Research*, vol. IV, edited by J. Biggens, Hijhoff Publ., Netherlands.
- Best, M. J., et al. (2011), The joint UK Land Environment Simulator (JULES), model description-Part 1: Energy and water fluxes, *Geosci. Model Dev.*, *4*, 677–699, doi:10.5194/gmd-4-677-2011.
- Beven, K. J., and H. L. Clocke (2012), Comment on “Hyperresolution global land surface modeling: Meeting a grand challenge for monitoring Earth’s terrestrial water” by Eric F. Wood et al., *Water Resour. Res.*, *48*, W01801, doi:10.1029/2011WR010982.
- Beven, K. J., and M. J. Kirkby (1979), A physically based, variable contributing area model of basin hydrology, *Hydrol. Sci. J.*, *24*(1), 43–69.
- Bonan, G. B., S. Levis, L. Kergoat, and K. W. Oleson (2002), Landscapes as patches of plant functional types: An integrating concept for climate and ecosystem models, *Global Biogeochem. Cycles*, *16*(2), 1021, doi:10.1029/2000GB001360.
- Budyko, M. I. (1974), *Climate and Life*, Int. Geophys. Ser., English edition edited by David H. Miller, Academic, New York.
- Campbell, G. S. (1974), A simple method for determining unsaturated conductivity from moisture retention data, *Soil Sci.*, *117*, 311–314.
- Charney, J. G. (1975), Dynamics of deserts and drought in the Sahel, *Q. J. R. Meteorol. Soc.*, *101*, 193–202.
- Clapp, R. B., and G. M. Hornberger (1978), Empirical equations for some soil hydraulic properties, *Water Resour. Res.*, *14*(4), 601–604.
- Colello, G. D., C. Grivet, P. J. Sellers, and J. A. Berry (1998), Modeling of energy, water and CO₂ flux in a temperate grassland ecosystem with SiB2: May-October 1987, *J. Atmos. Sci.*, *55*, 1141–1169.
- Collatz, G. J., J. T. Ball, C. Grivet, and J. A. Berry (1991), Physiological and environmental regulation of stomatal conductance, photosynthesis and transpiration: A model that includes a laminar boundary layer, *Agric. For. Meteorol.*, *54*, 107–136.
- Collatz, G. J., M. Ribas-Carbo, and J. A. Berry (1992), Coupled photosynthesis-stomatal conductance model for leaves of C4 plants, *Aust. J. Plant Physiol.*, *19*(5), 519–538.
- Corbin, K. D., A. S. Denning, L. Lu, J. W. Wang, and I. T. Baker (2008), Possible representation errors in inversions of satellite CO₂ retrievals, *J. Geophys. Res.*, *113*, D02301, doi:10.1029/2007JD008716.
- Corbin, K. D., A. S. Denning, E. Y. Lokupitya, A. E. Schuh, N. L. Miles, K. J. Davis, S. Richardson, and I. T. Baker (2010), Assessing the impact of crops on regional CO₂ fluxes and atmospheric concentrations, *Tellus, Ser. B*, *62*, 521–532.

- Costa, M. H., M. C. Biajoli, L. Sanches, A. C. M. Malhado, L. R. Hutyra, H. R. da Rocha, R. G. Aguiar, and A. C. de Araújo (2010), Atmospheric versus vegetation controls of Amazonian tropical rain forest evapotranspiration: Are the wet and seasonally dry rain forests any different? *J. Geophys. Res.*, *115*, G04021, doi:10.1029/2009JG001179.
- Dai, Y., et al. (2003), The common land model, *Bull. Am. Meteorol. Soc.*, *84*(8), 1013–1023.
- da Rocha, H. R., H. C. Freitas, R. Rosolem, R. Juarez, R. N. Tannus, M. A. Ligo, O. M. R. Cabral, and M. A. F. Silva Dias (2002), Measurements of CO₂ exchange over a woodland savanna (Cerrado *Sensu strictu*) in southeast Brasil, *Biota Neotropica*, *2*(1), 11.
- da Rocha, H. R., et al. (2009), Patterns of water and heat flux across a biome gradient from tropical forest to savanna in Brazil, *J. Geophys. Res.*, *114*, G00B12, doi:10.1029/2007JG000640.
- DeGonçalves, L. G., et al. (2013), Overview of the large-scale biosphere-Atmosphere Experiment in Amazonia Data Model Intercomparison Project (LBA-DMIP), *Agric. For. Meteorol.*, *182–183*, 111–127, doi:10.1016/j.agrformet.2013.04.030.
- Denning, A. S., G. J. Collatz, C. Zhang, D. A. Randall, J. A. Berry, P. J. Sellers, G. D. Colello, and D. A. Dazlich (1996), Simulations of terrestrial carbon metabolism and atmospheric CO₂ in a general circulation model. Part 1: Surface carbon fluxes, *Tellus, Ser. B*, *48*, 521–542.
- Denning, A. S., M. Nicholls, L. Prihodko, I. Baker, P.-L. Vidale, K. Davis, and P. Bakwin (2002), Simulated and observed variations in atmospheric CO₂ over a Wisconsin forest using a coupled Ecosystem-Atmosphere Model, *Global Change Biol.*, *9*, 1241–1250.
- Entekhabi, D., and P. S. Eagleson (1989), Land surface hydrology parameterization for atmospheric general circulation models including subgrid scale spatial variability, *J. Clim.*, *2*, 816–831.
- Entekhabi, D., I. Rodriguez-Iturbe, and F. Castelli (1996), Mutual interaction of soil moisture state and atmospheric processes, *J. Hydrol.*, *184*, 3–17.
- Famiglietti, J. S., and E. F. Wood (1994a), Multiscale modeling of spatially variable water and energy balance processes, *Water Resour. Res.*, *30*(11), 3061–3078.
- Famiglietti, J. S., and E. F. Wood (1994b), Application of multiscale water and energy balance models on a tallgrass prairie, *Water Resour. Res.*, *30*(11), 3079–3093.
- Famiglietti, J. S., J. A. Devereaux, C. A. Laymon, T. Tsegaye, P. R. Houser, T. J. Jackson, S. T. Graham, M. Rodell, and P. J. van Oevelen (1999), Ground-based investigation of soil moisture variability within remote sensing footprints during the Southern Great Plains 1997 (SGP97) hydrology experiment, *Water Resour. Res.*, *35*(6), 1839–1851.
- Farquhar, G. D., S. von Caemmerer, and J. A. Berry (1980), A biochemical model of photosynthetic CO₂ assimilation in leaves of C3 species, *Planta*, *149*, 78–90.
- Fischer, M. L., D. P. Billesbach, J. A. Berry, W. J. Riley, and M. S. Torn (2007), Spatiotemporal variations in growing season exchanges of CO₂, H₂O, and sensible heat in agricultural fields of the southern great plains, *Earth Interact.*, *11*, 17, doi:10.1175/EI231.1.
- Gentine, P., P. D'Odorico, B. R. Lintner, G. Sivandran, and G. Salvucci (2012), Interdependence of climate, soil, and vegetation as constrained by the Budyko curve, *Geophys. Res. Lett.*, *39*, L19404, doi:10.1029/2012GL053492.
- Georgi, F., and R. Avissar (1997), Representation of heterogeneity effects in earth system modeling: Experience from land surface modeling, *Rev. Geophys.*, *35*, 413–438.
- Goulden, M. L., S. D. Miller, H. R. da Rocha, M. C. Menton, H. C. de Freitas, A. M. E. Silva Figueira, and C. A. D. de Sousa (2004), Diel and seasonal patterns of tropical forest CO₂ exchange, *Ecol. Appl.*, *14*(4), S42–S54.
- Hanan, N. P., J. A. Berry, S. B. Verma, E. A. Walter-Shea, A. E. Suyker, G. G. Burba, and A. S. Denning (2005), Testing a model of CO₂, water and energy exchange in great plains tallgrass prairie and wheat ecosystems, *Agric. For. Meteorol.*, *31*, 162–179.
- Jackson, R. B., J. Canadell, J. R. Ehleringer, H. A. Mooney, O. E. Sala, and E. D. Schulze (1996), A global analysis of root distributions for terrestrial biomes, *Oecologia*, *180*(3), 389–411.
- Ke, Y., L. R. Leung, M. Huang, and H. Li (2013), Enhancing the representation of subgrid land surface characteristics in land surface models, *Geosci. Model Dev.*, *6*, 1609–1622, doi:10.5194/gmd-6-1609-2013.
- Kim, T.-H., M. Böhmer, H. Hu, N. Nishimur, and J. I. Schroeder (2010), Guard cell signal transduction network: Advances in understanding Abscisic acid, CO₂, and Ca²⁺ signaling, *Annu. Rev. Plant Biol.*, *61*, 561–591, doi:10.1146/annurev-arplant-042809-112226.
- Koster, R. D., and M. J. Suarez (1992), Modeling the land surface boundary in climate models as a composite of independent vegetation stands, *J. Geophys. Res.*, *97*(D3), 2697–2715.
- Koster, R. D., M. J. Suarez, A. Ducharme, M. Steiglitz, and P. Kumar (2000), A catchment-based approach to modeling land surface processes in a general circulation model 1. Model structure, *J. Geophys. Res.*, *105*(D20), 24,809–24,822.
- Koster, R. D., et al. (2004), Regions of strong coupling between soil moisture and precipitation, *Science*, *305*, 1138–1140, doi:10.1126/science.1100217.
- Koster, R. D., et al. (2006), GLACE: The Global Land-Atmosphere Coupling Experiment. Part I: Overview, *J. Hydrometeorol.*, *7*, 590–610.
- Krinner, G., N. Viovy, N. de Noblet-Ducoudré, J. Ogee, J. Polcher, P. Friedlingstein, P. Ciais, S. Sitch, and I. C. Prentice (2005), A dynamic global vegetation model for studies of the coupled atmosphere-biosphere system, *Global Biogeochem. Cycles*, *19*, GB1015, doi:10.1029/2003GB002199.
- Lawrence, D. M., et al. (2011), Parameterization improvement and functional and structural advances in version 4 of the Community Land Model, *J. Adv. Model. Earth Syst.*, *3*, M03001, doi:10.1029/2011MS000045.
- Laio, F., A. Porporato, L. Ridolfi, and I. Rodriguez-Iturbe (2001a), Plants in water-controlled ecosystems: Active role in hydrologic processes and response to water stress II. Probabilistic soil moisture dynamics, *Adv. Water Resour.*, *24*, 707–723.
- Laio, F., A. Porporato, C. P. Fernandez-Illescas, and I. Rodriguez-Iturbe (2001b), Plants in water-controlled ecosystems: Active role in hydrologic processes and response to water stress IV. Discussion of real cases, *Adv. Water Resour.*, *24*, 745–762.
- Li, B., and M. Rodell (2013), Spatial variability and its scale dependency of observed and modeled soil moisture over different climate regions, *Hydrol. Earth Syst. Sci.*, *17*, 1177–1188, doi:10.5194/hess-17-1177-2013.
- Liu, G., Y. Liu, and S. Endo (2013), Evaluation of surface flux parameterizations with long-term ARM observations, *Mon. Weather Rev.*, *141*, 773–797, doi:10.1175/MWR-D-12-00095.1.
- Liu, W., X. Xu, and G. Kiely (2012), Spatial variability of remotely sensed soil moisture in a temperate-humid grassland catchment, *Ecohydrology*, *5*, 668–676, doi:10.1002/cco.254.
- Lowry, W. P. (1959), The falling rate phase of evaporative soil-moisture loss—A critical evaluation, *Bull. Am. Meteorol. Soc.*, *40*(12), 605–608.
- Medina, I. D., A. S. Denning, I. T. Baker, J. A. Ramirez, and D. A. Randall (2014), A sampling method for improving the representation of spatially varying precipitation and soil moisture using the Simple Biosphere Model, *J. Adv. Model. Earth Syst.*, *6*, 9–20, doi:10.1002/2013MS000251.
- Muchow, R. C., and T. R. Sinclair (1991), Water deficit effects on Maize yields modeled under current and “greenhouse” climates, *Agron. J.*, *83*(6), 1052–1059.

- Nakaegawa, T., T. Oki, and K. Musiak (2000), The effects of heterogeneity within an area on areally averaged evaporation, *Hydrol. Processes*, *14*, 465–479.
- Nicholls, M. E., A. S. Denning, L. Prihodko, P.-L. Vidale, I. T. Baker, K. Davis, and P. Bakwin (2004), A multiple-scale simulation of variations in atmospheric carbon dioxide using a coupled biosphere-atmosphere model, *J. Geophys. Res.*, *109*, D18117, doi:10.1029/2003JD004482.
- ORNL DAAC (2008a), *MODIS Collection 5 Land Products Global Subsetting and Visualization Tool*, Oak Ridge, Tenn. Subset obtained for MOD15A2 product at 21.6185,47.650°W, time period: 2001-01-01 to 2003-12-31, and subset size: 0.25 x 0.25 km, doi:10.3334/ORNL-DAAC/1241.
- ORNL DAAC (2008b), *MODIS Collection 5 Land Products Global Subsetting and Visualization Tool*, Oak Ridge, Tenn. Subset obtained for MOD15A2 product at 36.605N,97.485°W, time period: 2000-01-01 to 2007-12-31, and subset size: 0.25 x 0.25 km, doi:10.3334/ORNL-DAAC/1241.
- Pan, Y.-X., X.-P. Wang, R.-L. Jia, Y.-W. Chen, and M.-Z. He (2008), Spatial variability of surface soil moisture content in a re-vegetated desert area in Shapotou, Northern China, *J. Arid Environ.*, *72*, 1675–1683, doi:10.1016/j.jaridenv.2008.03.010.
- Pierce, L. T. (1958), Estimating seasonal and short-term fluctuations in evapo-transpiration from meadow crops, *Bull. Am. Meteorol. Soc.*, *39*(2), 73–78.
- Pitman, A. J. (2003), The evolution of, and revolution in, land surface schemes designed for climate models, *Int. J. Climatol.*, *23*, 479–510, doi:10.1002/joc.893.
- Porporato, A., F. Laio, L. Ridolfi, and I. Rodriguez-Iturbe (2001), Plants in water-controlled ecosystems: Active role in hydrologic processes and response to water stress III. Vegetation water stress, *Adv. Water Resour.*, *24*, 725–744.
- Porporato, A., P. D'Odorico, F. Laio, L. Ridolfi, and I. Rodriguez-Iturbe (2002), Ecohydrology of water-controlled ecosystems, *Adv. Water Resour.*, *25*, 1335–1348.
- Randall, D. A., et al. (1996), A revised land surface parameterization (SiB2) for GCMs. Part III: The Greening of the Colorado State University General Circulation Model, *J. Clim.*, *9*(4), 738–763.
- Raz-Yaseef, N., D. Billesbach, M. L. Fischer, S. C. Biraud, S. A. Gunter, J. A. Bradford, and M. S. Torn (2015), Vulnerability of crops and native grasses to summer drying in the U.S. Southern Great Plains, *Agric. Ecosyst. Environ.*, *213*, 209–218, doi:10.1016/j.agee.2015.07.021.
- Restrepo-Coupe, N., et al. (2013), What drives the seasonality of photosynthesis across the Amazon basin? A cross-site analysis of eddy flux tower measurement from the Brasil flux network, *Agric. For. Meteorol.*, *182–183*, 128–144, doi:10.1016/j.agrformet.2013.04.031.
- Rodriguez-Iturbe, I. (2000), Ecohydrology: A hydrologic perspective of climate-soil-vegetation dynamics, *Water Resour. Res.*, *36*(1), 3–9.
- Ryu, D., and J. S. Famiglietti (2006), Multi-scale spatial correlation and scaling behavior of surface soil moisture, *Geophys. Res. Lett.*, *33*, L08404, doi:10.1029/2006GL025831.
- Santanello, J. A., and C. D. Peters-Lidard (2011), Diagnosing the sensitivity of local land-atmosphere coupling via the soil moisture-boundary layer interaction, *J. Hydrometeorol.*, *12*, 766–786, doi:10.1175/JHM-D-10-05014.1.
- Sato, N. P., J. Sellers, D. A. Randall, E. K. Schneider, J. Shukla, J. L. Kinter, Y. T. Hou, and E. Albertazzi (1989), Effects of implementing the simple biosphere model in a general circulation model, *J. Atmos. Sci.*, *46*(18), 2757–2782.
- Schaefer, K., G. J. Collatz, P. Tans, A. S. Denning, I. Baker, J. Berry, L. Prihodko, N. Suits, and A. Philpott (2008), The combined Simple Biosphere/Carnegie-Ames-Stanford Approach (SiBCASA) terrestrial carbon cycle model, *J. Geophys. Res.*, *113*, G03034, doi:10.1029/2007JG000603.
- Schmugge, T. J., and T. J. Jackson (1996), Soil moisture variability, in *Scaling Up in Hydrology Using Remote Sensing*, pp. 183–192, John Wiley, New York.
- Schwalm, C., et al. (2010), A model-data intercomparison of CO₂ exchange during a large scale drought event: Results from the North American Carbon Program Site Synthesis, *J. Geophys. Res.*, *115*, G00H05, doi:10.1029/2009JG001229.
- Sellers, P. J., Y. Mintz, Y. C. Sud, and A. Dalcher (1986), A Simple Biosphere Model (SiB) for use within general circulation models, *J. Atmos. Sci.*, *43*(6), 505–531.
- Sellers, P. J., M. D. Heiser, and F. G. Hall (1992a), Relations between surface conductance and spectral vegetation indices at intermediate (100 m² to 15 km²) length scales, *J. Geophys. Res.*, *97*(D17), 19,033–19,059.
- Sellers, P. J., J. A. Berry, G. J. Collatz, C. B. Field, and F. G. Hall (1992b), Canopy reflectance, photosynthesis, and transpiration. III. A reanalysis using improved leaf models and a new canopy integration scheme, *Remote Sens. Environ.*, *42*, 187–216.
- Sellers, P. J., M. D. Heiser, F. G. Hall, S. J. Goetz, D. E. Strebel, S. B. Verma, R. L. Desjardins, P. M. Scheupp, and J. I. MacPherson (1995), Effects of spatial variability in topography, vegetation cover and soil moisture on area-averaged surface fluxes: A case study using the FIFE 1989 data, *J. Geophys. Res.*, *100*(D12), 25,607–25,629.
- Sellers, P. J., D. A. Randall, G. J. Collatz, J. A. Berry, C. B. Field, D. A. Dazlich, C. Zhang, G. D. Collelo, and L. Bounoua (1996a), A Revised Land Surface Parameterization (SiB2) for atmospheric GCMs. Part I: Model formulation, *J. Clim.*, *9*(4), 676–705.
- Sellers, P. J., S. O. Los, C. J. Tucker, C. O. Justice, D. A. Dazlich, G. J. Collatz, and D. A. Randall (1996b), A Revised Land Surface Parameterization (SiB2) for atmospheric GCMs. Part II: The generation of global fields of terrestrial biophysical parameters from satellite data, *J. Clim.*, *9*(4), 706–737.
- Sellers, P. J., L. Bounoua, G. J. Collatz, D. A. Randall, D. A. Dazlich, S. O. Los, J. A. Berry, I. Fung, C. J. Tucker, C. B. Field, and T. G. Jensen (1996c), Comparison of radiative and physiological effects of doubled atmospheric CO₂ on climate, *Science*, *271*, 1402–1406.
- Sellers, P. J., et al. (1997), Modeling the exchanges of energy, water, and carbon between continents and the atmosphere, *Science*, *275*, 502–509.
- Sellers, P. J., M. J. Fennessy, and R. E. Dickinson (2007), A numerical approach to calculating soil wetness and evapotranspiration over large grid areas, *J. Geophys. Res.*, *112*, D18106, doi:10.1029/2007JD008781.
- Serraj, R., L. H. Allen, and T. P. Sinclair (1999), Soybean leaf growth and gas exchange response to drought under carbon dioxide enrichment, *Global Change Biol.*, *5*, 283–291.
- Seneviratne, S. I., T. Corti, E. L. Davin, M. Hirschi, E. B. Jaeger, I. Lehner, B. Orlowsky, and A. J. Teuling (2010), Investigating soil moisture-climate interactions in a changing climate: A review, *Earth Sci. Rev.*, *99*, 125–161, doi:10.1016/j.earscirev.2010.02.004.
- Shukla, J., and Y. Mintz (1982), Influence of land-surface evapotranspiration on the Earth's climate, *Science*, *215*, 1498–1501.
- Shuttleworth, W. J. (1988), Macrohydrology—The new challenge for process hydrology, *J. Hydrol.*, *100*, 31–56.
- Sivapalan, M., K. Beven, and E. F. Wood (1987), On hydrologic similarity 2. A scaled model of storm runoff production, *Water Resour. Res.*, *23*(12), 2266–2278.
- Teuling, A. J., F. Hupet, R. Uijlenhoet, and P. A. Troch (2007), Climate variability effects on spatial soil moisture dynamics, *Geophys. Res. Lett.*, *34*, L06406, doi:10.1029/2006GL029080.

- Wang, J.-W., A. S. Denning, L. Lu, I. T. Baker, K. D. Corbin, and K. J. Davis (2007), Observations and simulations of synoptic, regional, and local variations in atmospheric CO₂, *J. Geophys. Res.*, *112*, D04108, doi:10.1029/2006JD007410.
- Wood, E. F., M. Sivapalan, K. Beven, and L. Band (1988), Effects of spatial variability and scale with implications to hydrologic modeling, *J. Hydrol.*, *102*, 29–47.
- Wood, E. F., D. P. Lettenmeier, and V. G. Zartarian (1992), A land-surface hydrology parameterization with subgrid variability for general circulation models, *J. Geophys. Res.*, *97*(D3), 2717–2728.
- Wood, E. F., et al. (2011), Hyperresolution global land surface modeling: Meeting a grand challenge for monitoring Earth's terrestrial water, *Water Resour. Res.*, *47*, W05301, doi:10.1029/2010WR010090.
- Yang, Z.-L. (2004), Modeling land surface processes in short-term weather and climate studies, in *Observations, Theory, and Modeling of Atmospheric Variability, Ser. Meteorol. East Asia*, vol. 3, edited by X. Zhu, pp. 288–313, World Sci., Singapore.